

Antiferromagnetism, f -wave and chiral p -wave superconductivity in a Kagome lattice with possible application to sd^2 -graphenes

Wan-Sheng Wang,^{1,2} Yuan-Chun Liu,¹ Yuan-Yuan Xiang,³ and Qiang-Hua Wang^{1,4}

¹*National Laboratory of Solid State Microstructures & School of Physics, Nanjing University, Nanjing, 210093, China*

²*Department of Physics, Ningbo University, Ningbo 315211, China*

³*College of Science, Hehai University, Nanjing, 210098, China*

⁴*Collaborative Innovation Center of Advanced Microstructures, Nanjing 210093, China**

We investigate the electronic instabilities in a Kagome lattice with Rashba spin-orbital coupling by the unbiased singular-mode functional renormalization group. At the parent $1/3$ -filling, the normal state is a quantum spin Hall system. Since the bottom of the conduction band is near the van Hove singularity, the electron-doped system is highly susceptible to competing orders upon electron interactions. The topological nature of the parent system enriches the complexity and novelty of such orders. We find 120° -type intra-unitcell antiferromagnetic order, f -wave superconductivity and chiral p -wave superconductivity with increasing electron doping above the van Hove point. In both types of superconducting phases, there is a mixture of comparable spin singlet and triplet components because of the Rashba coupling. The chiral p -wave superconducting state is characterized by a Chern number $Z = 1$, supporting a branch of Weyl fermion states on each edge. The model bares close relevance to the so-called sd^2 -graphenes proposed recently.

PACS numbers: 71.10.Fd, 74.20.-z, 74.20.Rp, 71.27.+a

I. INTRODUCTION

The Kagome lattice systems have attracted considerable attentions due to the rich physics associated with the high degree of geometrical frustration. In the Mott insulating limit, several possible states have been proposed as the ground states of the Heisenberg model in this lattice, such as a valance bond solid state (with 36 sites per unit cell),¹⁻⁵ a $U(1)$ algebraic spin liquid (SL),⁶ a disordered triplet gapped SL,⁷ and a singlet gapped SL with signatures of Z_2 topological order and anyonic excitations.⁸⁻¹⁰ At low hole doping, a special valance bond crystal state (with 12 sites per unit cell) is proposed as the ground state of the t - J model in this lattice.^{11,12} For intermediate interactions and at various fillings, several exotic phases have been proposed for the Kagome lattice, such as peculiar Mott transition,^{13,14} anomalous quantum Hall effects,^{15,16} and semionic states at half filling,¹⁷ fractional charge at $1/3$ filling for spinless fermions,¹⁸ and ferromagnetism at electron filling $1/3$ (or $5/3$).¹⁹

There are also extensive interests in the itinerant limit of the Kagome lattice. In particular, at the van Hove filling, the Fermi surface (FS) is perfectly nested and has saddle points on the edges of the Brillouine Zone (BZ). This would make the system unstable against weak interactions. Similar FS appears in triangle and honeycomb lattices and was shown to develop a chiral spin-density-wave (SDW),²⁰⁻²² or a chiral $d_{x^2-y^2} + id_{xy}$ pairing.^{23,24} Both states break time-reversal and parity symmetries and are topologically nontrivial. Given the similar FS, a simple FS nesting argument would predict similar orders in the Kagome lattice. However, the character of the Bloch state on the FS depends on the position of the momentum. The nesting vector connects two Bloch states with different sublattice contents, weakening the nesting effect as far as an on-site interaction U is concerned.²⁵⁻²⁷

Such a matrix element effect causes profound difference to the case of honeycomb lattice. At the van Hove filling, the instabilities are ferromagnetism, intra-unitcell antiferromagnetism and charge-bond-order (CBO) with increasing U .²⁷ There is a concern on the fate of the ferromagnetic order in the limit of large U .²⁸ However, such an order is unlikely as viewed from the equivalent t - J model, which supports the CBO instead.¹² In addition, the nearest-neighbor (NN) repulsion V connects different sublattices and thus enjoys the FS nesting, leading to additional instabilities. For example, the $d_{x^2-y^2} + id_{xy}$ pairing and spin-bond-order appear if V and U are comparable, while the charge-density-wave (CDW) and s -wave pairing are found if V dominates.²⁷

The orders mentioned so far are found in the absence of spin-orbital coupling (SOC). We ask how would SOC modify or enrich the orders. We are motivated by the fact that SOC could cause nontrivial topology already at the single-particle level. In the Kane-Mele model, the Rashba-type SOC connecting next-nearest-neighbor (NNN) bonds of the honeycomb lattice, and makes the system at half filling a quantum spin Hall (or a two-dimensional topological insulator). However, in a realistic system such as graphene, the SOC is too small to be practical. Apart from the lightness of the carbon atom, the weakness of SOC in graphene arises from the fact that the SOC connects the longer NNN bond about which the two sides are asymmetric. In Kagome lattice, however, there is an asymmetry already about the NN bond. It is therefore more hopeful to look for SOC in Kagome lattices. Interestingly, such a material is indeed proposed from first principle. It is a honeycomb lattice of transition metal (TM) atoms, but the low energy electrons are described effectively by Kagome bands.²⁹ This is because the sd^2 -hybridized σ -orbitals are bond-centered on the honeycomb lattice, so that electrons hop effectively on

the Kagome lattice dual to the honeycomb lattice. The TM atoms display large Rashba-type SOC. Such a system is dubbed sd^2 -graphene. The system displays magnetism (from local moment due to unsaturated lower atomic levels) for the TM element W , enabling quantum anomalous Hall effect.²⁹ The calculation also shows that the atomic magnetism could be avoided for other TM elements. Here we are interested in the latter case, as we are concerned mainly on the superconducting order, which would be unlikely stable against the strong local spin exchange. We notice that in the parent sd^2 -graphene (at the $1/3$ filling), the bottom of the conduction band above the band gap is rather flat and close to the van Hove point. Therefore by slight electron doping the system would be highly susceptible to competing orders upon electron interactions. The topological nature of the parent system would enrich the complexity and novelty of such orders.

In this paper, we investigate the electronic instabilities of electron doped sd^2 -graphene near the van Hove filling. To treat the correlation effects in an unbiased way, we resort to the singular-mode functional renormalization group (SMFRG) developed recently.^{22,30,31} We find intracell antiferromagnetism (AFM), f -wave and chiral $p + ip$ -wave superconductivity (SC), with increasing deviation from the van Hove level. In both types of superconducting phases, there is a mixture of comparable spin singlet and triplet components because of the Rashba coupling. The chiral p -wave superconducting state is characterized by a Chern number $Z = 1$, supporting a branch of Weyl fermion states on each edge.

The rest of the paper is arranged as follows. In Sec.II, we define the model and briefly introduce the SMFRG method. In Sec.III, we discuss the results for various electron doping levels and present the phase diagram. Finally, Sec.IV is a summary and perspective of this work.

II. MODEL AND METHOD

The structure of sd^2 -graphene is schematically shown in Fig.1(a), where the red circles and red-dashed lines show the position of TM atoms and the corresponding honeycomb lattice. For TM atoms, the s , d_{xy} and $d_{x^2-y^2}$ orbitals hybridize to form bonding σ -orbitals around the centers of the NN bonds on the honeycomb lattice, shown as solid blue circles in Fig.1(a), as well as antibonding σ^* -orbitals at higher energy beyond the present interest. In contrast to the π -orbitals in graphene, the bond-centered σ -orbitals form effectively a Kagome lattice (dual to the honeycomb lattice), shown as the blue solid lines in Fig.1(a), with three sublattices α , β , and γ . The effective Hamiltonian derived from the σ -orbitals is given by²⁹

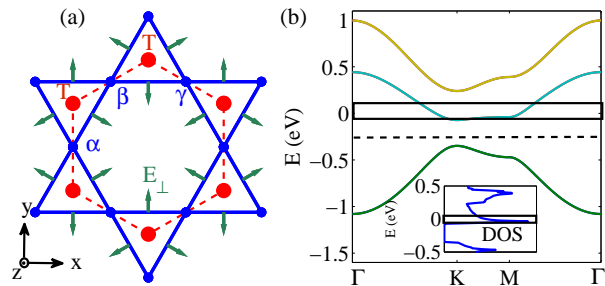


FIG. 1: (Color online) (a) The structure of sd^2 -graphene. The TM atoms (red circles) are located on the honeycomb lattice (red dashed lines). The σ orbitals (blue circles) define a Kagome lattice (blue lines), with three sublattices α , β and γ . The arrows show the crystal electric field E_{\perp} on the NN bonds of the Kagome lattice. The spatial axes are defined by x , y and z . (b) The band structure of the effective model. The dashed line indicates the Fermi level for the parent $1/3$ filling. The black rectangle shows the electron doping regime under concern. There is a van Hove singularity with large density of states near the bottom of the conduction band (inset).

$$H = - \sum_{\langle ij \rangle \sigma} (c_{i\sigma}^{\dagger} t_{ij} c_{j\sigma} + \text{h.c.}) - \mu \sum_{i\sigma} n_{i\sigma} + U \sum_i n_{i\uparrow} n_{i\downarrow} + \frac{i\lambda}{2} \sum_{\langle ij \rangle \in \text{NN}, \sigma} (c_{i\sigma}^{\dagger} \sigma \eta_{ij} c_{j\sigma} - \text{h.c.}) \quad (1)$$

Here $c_{i\sigma}^{\dagger}$ creates an electron with spin $\sigma = \pm 1$, μ is the chemical potential, and $\langle ij \rangle$ denotes the bonds between the first, second and third neighbors (henceforth on Kagome lattice), with the corresponding hopping integrals $t_{1,2,3}$. The Rashba SOC on the NN bonds is given by λ in strength, and $\eta_{ij} = \pm 1$ is the sign of $\hat{z} \cdot (\mathbf{E}_{ij} \times \mathbf{R}_{ij})$, where \mathbf{E}_{ij} is the crystal electric field, depicted as arrows in Fig.1(a), and $\mathbf{R}_{ij} = \mathbf{r}_i - \mathbf{r}_j$ is the displacement vector during electron hopping.

For concreteness, we set $t_1 = 0.25\text{eV}$, $t_2 = 0.05\text{eV}$, and $t_3 = -0.02\text{eV}$ and we set Rashba SOC $\lambda = 0.16\text{eV}$, as it is found strong in Ref.²⁹. (Our results do not change qualitatively against fine tuning of these parameters, as will be discussed in the end of section III.) The corresponding band structure is shown in Fig.1(b). Notice that each band is two-fold degenerate even in the presence of the SOC in Eq.1. At the parent $1/3$ filling, the Fermi level lies between the lower two bands. We are interested in electron doping above the van Hove singularity in the conduction band. We should emphasize that the hopping integrals may depend on the TM atoms, but the existence of a van Hove point near the bottom of the conduction band is quite general. On the other hand, the doping level can be controlled by TM substitution, adsorption of alkaline atoms, or electric gating.

We treat the effect of the Coulomb interaction U by SMFRG.^{22,30,31} A general four-point interaction vertex

Γ can be decomposed as

$$\Gamma = \sum_{\mathbf{q}\nu} (A_{\mathbf{q}}^{\nu})^{\dagger} S^{\nu}(\mathbf{q}) A_{\mathbf{q}}^{\nu}, \quad (2)$$

where ν denotes an eigenmode of Γ , \mathbf{q} is a collective momentum, and $A_{\mathbf{q}}^{\nu}$ is a composite boson field made up of a fermion bilinear. In the particle-particle (pp) channel, $(A_{\mathbf{q}}^{\nu})^{\dagger} = \sum_{\mathbf{k}} \psi_{\mathbf{k}+\mathbf{q}}^{\dagger} \phi_{\mathbf{q}}^{\nu}(\mathbf{k}) (\psi_{-\mathbf{k}}^{\dagger})^T$, while in the particle-hole (ph) channel, $(A_{\mathbf{q}}^{\nu})^{\dagger} = \sum_{\mathbf{k}} \psi_{\mathbf{k}+\mathbf{q}}^{\dagger} \phi_{\mathbf{q}}^{\nu}(\mathbf{k}) \psi_{\mathbf{k}}$. Here $\psi_{\mathbf{k}}$ is a six-component spinor in the momentum space, made of $c_{\mathbf{k}\sigma a}$ for $\sigma = \pm$ and $a = \alpha, \beta$ and γ . The inner structure of the composite boson is described by a matrix form factor $\phi_{\mathbf{q}}^{\nu}(\mathbf{k})$. The decompositions of the same interaction vertex into pp and ph channels imply that there are overlaps between them, which are handled on equal footing in the SMFRG. We also emphasize that SMFRG takes all bands into account, since it works in the orbital rather than band basis. Starting from the bare interaction vertex given by the U -term in Eq.1, the effective vertex Γ flows versus a decreasing infrared cutoff energy scale Λ . We monitor the associated evolution of $S_{pp,ph}^{\nu}(\mathbf{q})$ as well as the form factors. The most negative (i.e., attractive) $S_{pp,ph}^{\nu}(\mathbf{q})$ indicates the leading mode in the respective channel, which we denote as $S_{pp,ph}$ for brevity. A diverging leading mode implies an instability of the normal state, and the associated collective momentum \mathbf{Q} and form factor $\phi(\mathbf{k})$ (dropping the collective momentum and the mode index) describe the emerging order parameter. The divergence energy scale is an upper limit of the transition temperature T_c . More technical details can be found elsewhere.^{22,30-32}

III. RESULTS AND DISCUSSIONS

In this section, we provide the SMFRG results for the model defined in the previous section. We begin by discussing the results for specific fillings (chemical potentials) with $U = 1\text{eV}$, and summarize the results by a phase diagram in the (U, μ) space.

Intra-unit-cell antiferromagnetism: We first consider the case of van Hove filling at which $\mu = -0.04\text{eV}$. The FRG flow versus the running energy scale Λ is shown in Fig.2(a). Clearly, the ph channel is leading. We find that the associated collective momentum is $\mathbf{Q} = 0$, and the form factor $\phi(\mathbf{k})$ is given by, up to a global $\text{SO}(2)$ symmetry within the xy -plane,

$$(\phi^{\alpha\alpha}, \phi^{\beta\beta}, \phi^{\gamma\gamma}) = (-\sigma_y, \frac{\sigma_y + \sqrt{3}\sigma_x}{2}, \frac{\sigma_y - \sqrt{3}\sigma_x}{2}), \quad (3)$$

where $\sigma_{x,y,z}$ are Pauli matrices in the spin basis. (The other elements are essentially zero.) The form factor is diagonal in sublattice basis and independent of \mathbf{k} , meaning the order is site-local. On the other hand, the spin dependence indicates that the order is in the spin sector, and moreover the angle between nearby spins is 120° .

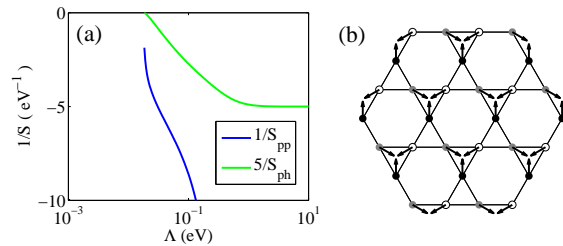


FIG. 2: (Color online) Results for $\mu = -0.04\text{eV}$. (a) FRG flow of (the inverse of) the most negative singular values S in the particle-particle (pp) and particle-hole (ph) channels. (b) the spin structure of the leading mode in ph channel.

Finally, $\mathbf{Q} = 0$ means the spin ordering is ferromagnetic in terms of translation by unit cells. The corresponding spin structure is shown in Fig.2(b), which we call an intra-unitcell AFM. This $\mathbf{Q} = 0$ instability in the ph channel is clearly enhanced by the van Hove singularity rather than FS nesting, as a result of the matrix element effect discussed previously. It also appears even if the SOC is absent.²⁷

f-wave superconductivity: Now we consider a slightly higher electron doping with $\mu = -0.005\text{eV}$. The FS is shown in Fig.3(a), and Fig.3(b) shows the FRG flow. In the present case, the ph channel is enhanced at higher energy scales, but saturates at low energy scales due to lack of phase space for low energy particle-hole excitations in the absence of perfect nesting. On the other hand, the pp channel is triggered attractive (even though the initial interaction is repulsive) while the ph channel is enhanced, a manifestation of the channel overlap. At still lower energy scales, the pp channel (at $\mathbf{Q} = 0$) can diverge on its own due to the Cooper instability mechanism. Therefore, the system will develop superconductivity below the divergence energy scale. The form factor in this case is just the pairing function, which can be written as $\phi(\mathbf{k}) = (g_{\mathbf{k}} + d_{\mathbf{k}}\sigma_z) i\sigma_y$ in our case, with a singlet part $g_{\mathbf{k}}$ and a triplet part $d_{\mathbf{k}}$. (The ‘d-vector’ is always oriented along z .) The non-zero elements of $g_{\mathbf{k}}$ and $d_{\mathbf{k}}$ are given by

$$\begin{aligned} g_{\mathbf{k}}^{\alpha\beta} &= -g_{\mathbf{k}}^{\beta\alpha} = -i\Delta_s \sin \frac{k_+}{2}, \\ g_{\mathbf{k}}^{\alpha\gamma} &= -g_{\mathbf{k}}^{\gamma\alpha} = i\Delta_s \sin \frac{k_-}{2}, \\ g_{\mathbf{k}}^{\beta\gamma} &= -g_{\mathbf{k}}^{\gamma\beta} = i\Delta_s \sin \frac{k_x}{2}, \\ d_{\mathbf{k}}^{\alpha\alpha} &= \Delta_{t1} (\sin k_+ + \sin k_-) + \Delta_{t2} \sin k_x, \\ d_{\mathbf{k}}^{\beta\beta} &= \Delta_{t1} (\sin k_+ - \sin k_x) - \Delta_{t2} \sin k_-, \\ d_{\mathbf{k}}^{\gamma\gamma} &= \Delta_{t1} (\sin k_- - \sin k_x) - \Delta_{t2} \sin k_+, \end{aligned} \quad (4)$$

where $k_{\pm} = (k_x \pm \sqrt{3}k_y)/2$. Notice that the singlet/triplet part corresponds to pairing on the first/third neighbor bonds. We find that due to the SOC the singlet and triplet components are mixed with comparable ampli-

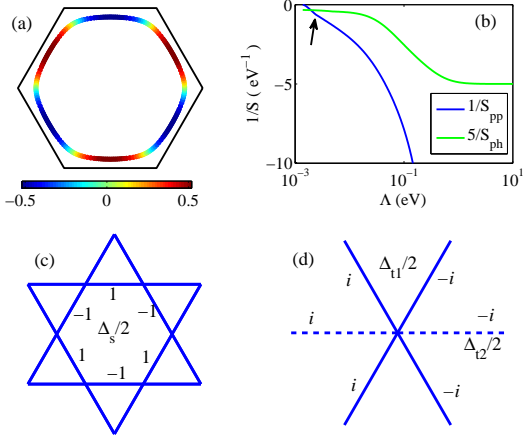


FIG. 3: (Color online) Results for $\mu = -0.005\text{eV}$. (a) The Fermi surface and the gap function (color scale) thereon. (b) FRG flow of (the inverse of) the most negative singular values S in the pp and ph channels. The arrow indicates a level crossing of the pairing modes. (c) Real-space pattern of singlet pairing on NN bonds. The phase factor is put on bonds and the amplitude is $\Delta_s/2$. (d) Real-space pattern of triplet pairing on third-neighbor bonds, starting from an α -site at the center. The amplitudes on solid (dashed) bonds are $\Delta_{t1}/2$ and $\Delta_{t2}/2$, respectively. The difference arises from the fact that the solid bond traverses a lattice site at the midpoint while the dashed one does not.

tudes $\Delta_s : \Delta_{t1} : \Delta_{t2} \sim 7 : 8 : 6$. Such a pairing configuration enjoys simultaneously the quasi-AFM correlation between nearby sublattices and FM correlation between like-sublattices (connected by the third-neighbor bonds), as discussed previously. The real-space pattern for the singlet and triplet parts are illustrated in Fig.3(c) and (d), respectively. By inspection, the singlet part transforms as f -wave with respect to the symmetry center (the center of the holo hexagon), which would be invalid without the sublattice structure. The same symmetry is carried by $d_{\mathbf{k}}$, guaranteed by group theory, but less obvious in Fig.3(d). To see this better, we transform the pairing function into the band basis, $\Delta_{\mathbf{k}} = \langle \mathbf{k} | \phi(\mathbf{k}) | \mathbf{k} \rangle$, where $|\mathbf{k}\rangle$ is a Bloch state (in the normal state) and $|\mathbf{k}\rangle = (T|\mathbf{k}\rangle)^*$, with T the time-reversal operator. The projected gap on the FS is shown in Fig.3(a), revealing explicitly the f -wave symmetry.

We remark that during the FRG flow, there is a level crossing in the pp channel at the energy scale indicated by the arrow in Fig.3(b). The leading pairing symmetry is p -wave/ f -wave above/below the crossing point. This implies the possibility of p -wave pairing if the filling level is tuned further.

$p + ip'$ -wave superconductivity. We consider further electron doping at $\mu = 0.02\text{eV}$. Fig.4(a) and (b) show the corresponding FS and the FRG flow. As in the previous case, the ph channel dominates at higher energy scales but saturates at lower scales, and the pp channel is triggered attractive by the ph channel, and in turn di-

verges eventually. We find that there are two degenerate pairing modes in the pp channel. Resolving the matrix pairing function as before, we find the dominant nonzero elements

$$\begin{aligned}
 g_{\mathbf{k}}^{\alpha\beta} &= -g_{\mathbf{k}}^{\beta\alpha} = -i\sqrt{3}\Delta_s \sin \frac{k_+}{2}, \\
 g_{\mathbf{k}}^{\alpha\gamma} &= -g_{\mathbf{k}}^{\gamma\alpha} = -i\sqrt{3}\Delta_s \sin \frac{k_-}{2}, \\
 d_{\mathbf{k}}^{\alpha\alpha} &= 2\Delta_t(\sin k_+ - \sin k_-), \\
 d_{\mathbf{k}}^{\beta\beta} &= \Delta_t(\sin k_x + \sin k_+), \\
 d_{\mathbf{k}}^{\gamma\gamma} &= -\Delta_t(\sin k_x + \sin k_-),
 \end{aligned} \tag{5}$$

for the first mode $\phi_1(\mathbf{k})$, and

$$\begin{aligned}
 g_{\mathbf{k}}^{\alpha\beta} &= -g_{\mathbf{k}}^{\beta\alpha} = -i\Delta_s \sin \frac{k_+}{2}, \\
 g_{\mathbf{k}}^{\alpha\gamma} &= -g_{\mathbf{k}}^{\gamma\alpha} = i\Delta_s \sin \frac{k_-}{2}, \\
 g_{\mathbf{k}}^{\beta\gamma} &= -g_{\mathbf{k}}^{\gamma\beta} = -2i\Delta_s \sin \frac{k_x}{2}, \\
 d_{\mathbf{k}}^{\beta\beta} &= \sqrt{3}\Delta_t(\sin k_x + \sin k_+), \\
 d_{\mathbf{k}}^{\gamma\gamma} &= \sqrt{3}\Delta_t(\sin k_x + \sin k_-)
 \end{aligned} \tag{6}$$

for the second mode $\phi_2(\mathbf{k})$. We find that $\Delta_s : \Delta_t \simeq 5 : 2$. So there is again a comparable mixture of singlets and triplets. We find $\phi_1(\mathbf{k})$ and $\phi_2(\mathbf{k})$ transform as p_x - and p_y -wave, respectively. As an example, we project $\phi_1(\mathbf{k})$ on the FS in Fig.4(a) (color scale), where the p_x -wave symmetry is apparent. The fact that the singlet part can transform as p -wave is again a consequence of the sublattice structure.

Since the two pairing modes are degenerate, additional analysis, such as the mean-field theory, is needed to fix the gap function in the ordered state. Given the explicit pairing functions from SMFRG, we are able to perform mean field calculations by the following effective hamiltonian, in the momentum space,

$$H_{MF} = H_0 + \sum_{\mathbf{k}, \nu} [\psi_{\mathbf{k}}^\dagger \Delta_\nu \phi_\nu(\mathbf{k}) (\psi_{-\mathbf{k}}^\dagger)^T + \text{h.c.}], \tag{7}$$

subject to the self-consistency,

$$\Delta_\nu = -g \langle (\psi_{-\mathbf{k}})^\dagger \phi_\nu^\dagger(\mathbf{k}) \psi_{\mathbf{k}} \rangle. \tag{8}$$

Here H_0 is the free part of H , Δ_ν is the order parameter for $\phi_\nu(\mathbf{k})$, and g is an effective coupling constant fixing the transition temperature at the FRG divergence scale. Notice that Δ_ν acts as the global amplitude for $\phi_\nu(\mathbf{k})$, so the coefficients $\Delta_{s,t}$ within $\phi_\nu(\mathbf{k})$ are fixed subject to the given ratio from FRG. Our mean-field calculation reveals that in the ordered state, the chiral combination $\phi_1(\mathbf{k}) \pm i\phi_2(\mathbf{k})$ is always favorable. The corresponding real-space pattern for the singlet part of the pairing function is shown in Fig.4(c). This could have been anticipated since both $\phi_1(\mathbf{k})$ and $\phi_2(\mathbf{k})$ have nodes on the FS, a nature way to gain energy is to form a $p \pm ip'$ -wave pairing, which gaps out the entire FS.

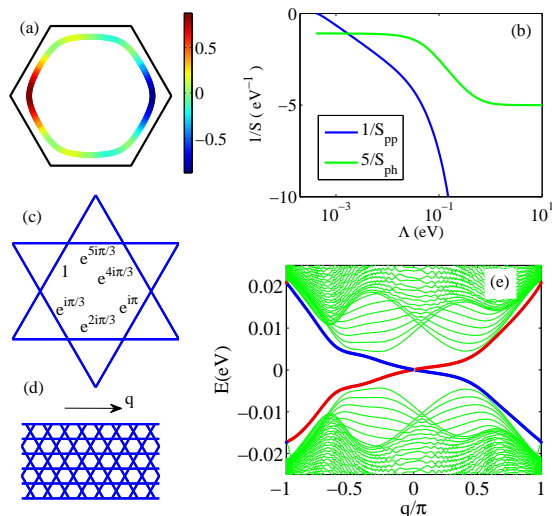


FIG. 4: (Color online) Results for $\mu = 0.02\text{eV}$. (a) The Fermi surface and the gap function (color scale) of one of the degenerate pairing modes thereon. (b) FRG flow of (the inverse of) the most negative singular values S in the pp and ph channels. (c) The real-space pattern of the singlet part in the $p + ip'$ pairing. (d) A strip of Kagome lattice periodic/open along the horizontal/vertical direction. Here q denotes the conserved momentum. (e) The low energy spectrum for (d) as a function of q . The red in-gap states are chiral modes on one edge, and the blue ones are on the other edge.

The chiral $p + ip'$ -pairing breaks time-reversal symmetry, and is topologically nontrivial. The topology is classified by the Chern number,³³

$$Z = \frac{1}{2\pi} \sum_n \int d^2\mathbf{k} (\partial_{k_x} A_y^n - \partial_{k_y} A_x^n) f(E_{n,\mathbf{k}}), \quad (9)$$

where n is a band index, $A_i^n = -i\langle n, \mathbf{k} | \partial_{k_i} | n, \mathbf{k} \rangle$ is the Berry connection, with $|n, \mathbf{k}\rangle$ an eigenstate of H_{MF} with energy $E_{n,\mathbf{k}}$, and finally f is the Fermi function at zero temperature. We find $Z = 1$, similarly to the case for the $p + ip'$ pairing in Sr_2RuO_4 .³⁴ To verify the topology of our superconducting state, we calculate the energy spectrum in a strip as shown in Fig.4(d). The energy spectrum as a function of the horizontal momentum q is shown in Fig.4(e). Within the bulk energy gap (which is artificially enlarged for a better view), there appear a branch of chiral states along each edge, in exact correspondence to $Z = 1$. Importantly, H_{MF} can be embedded, as we did here, in a Nambu space without redundant degrees of freedom. In this case each eigenstate describes a canonical fermion mode. Therefore the chiral edge states are best termed as one-dimensional Weyl (rather than Majorana) fermion modes.

The phase diagram: Apart from the typical results discussed above, we have performed systematic calculations

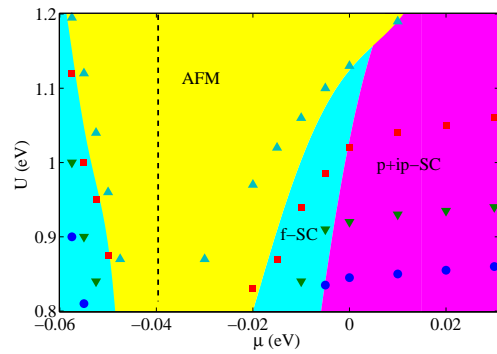


FIG. 5: (Color online) A schematic phase diagram of sd^2 -graphene in (U, μ) space. The dashed line highlights the van Hove level $\mu = -0.04\text{eV}$. The transition temperatures at some specific points of the phase diagram are 10meV (upper triangles), 1meV (squares), 0.1meV (lower triangles), and 0.01meV (circles).

for other values of U and other filling levels. The results are summarized as a schematic phase diagram in Fig.5. With increasing deviation from the van Hove filling, the system develops intra-unitcell AFM, f -wave and $p + ip'$ -wave SC. With increasing U , the fan of AFM increases, while the transition temperature (i.e., the divergence scale in FRG) also increases in all phases.

We find the phase diagram is not changed qualitatively for $0.06\text{eV} \leq \lambda \leq 0.16\text{eV}$, except that all the phase regimes are narrowed toward the van Hove filling if λ is reduced. The AFM survives down to $\lambda = 0$,²⁷ but the transition temperature for the SC states is too small to be of practical interest. On the other hand, the system develops a CBO at large U for $t_2 = t_3 = \lambda = 0$ due to the perfect nesting and matrix element effect.²⁷ This state does not appear here because the FS nesting is further degraded by t_2 and t_3 .

IV. SUMMARY AND PERSPECTIVE

We studied the electronic instabilities in electron-doped sd^2 -graphene. With increasing deviation from the van Hove filling, the system develops 120° -type non-collinear intra-unitcell AFM, f -wave and $p + ip'$ -wave SC states. In both SC states, singlets and triplets mix with comparable amplitudes due to SOC. The chiral $p + ip'$ -wave SC is characterized by a Chern number $Z = 1$, supporting a branch of Weyl fermion modes along each edge. Such modes can be probed by scanning tunneling microscopy, and would manifest itself as quantized thermal Hall conductivity.

Acknowledgments

The project was supported by NSFC (under grant Nos.11574134 and 11504085), the China Postdoctoral

Science Foundation (under Grant No.2014M561616) and the Fundamental Research Funds for the Central Univer-

sities (under grant No. 2014B14314).

-
- * Electronic address: qhwang@nju.edu.cn
- ¹ J. B. Marston and C. Zeng, *J. Appl. Phys.* **69**, 5962(1991).
 - ² R. R. P. Singh and D. A. Huse, *Phys. Rev. B.* **76**, 180407(2007).
 - ³ L. Balents, *Nature(London)* **464**, 199(2010).
 - ⁴ G. Evenbly and G. Vidal, *Phys. Rev. Lett.* **104**, 187203 (2010).
 - ⁵ D. Poilblanc, M. Mambrini, and D. Schwandt, *Phys. Rev. B* **81**, 180402(R) (2010).
 - ⁶ Y. Ran, M. Hermele, P. A. Lee, and X. G. Wen, *Phys. Rev. Lett.* **98**, 117205(2007).
 - ⁷ H. C. Jiang, Z. Y. Weng, and D. N. Sheng, *Phys. Rev. Lett.* **101**, 117203 (2008).
 - ⁸ S. Yan, D. A. Huse, and S. R. White, *Science* **332**, 1173 (2011).
 - ⁹ H. C. Jiang, Z. Wang, and L. Balents, *Nat. Phys.* **8**, 902 (2012).
 - ¹⁰ S. Depenbrock, I. P. McCulloch, and U. Schollwock, *Phys. Rev. Lett.* **109**, 067201 (2012).
 - ¹¹ S. Guertler and H. Monien, *Phys. Rev. B.* **84**, 174409 (2011).
 - ¹² S. Guertler and H. Monien, *Phys. Rev. Lett.* **111**, 097204 (2013).
 - ¹³ T. Ohashi, N. Kawakami, and H. Tsunetsugu, *Phys. Rev. Lett.* **97**, 066401(2006).
 - ¹⁴ A. Läuchli and D. Poilblanc, *Phys. Rev. Lett.* **92**, 236404(2004).
 - ¹⁵ K. Ohgushi, S. Murakami, and N. Nagaosa, *Phys. Rev. B* **62**, R6065(R) (2000).
 - ¹⁶ A. Petrescu, A. A. Houck, and K. Le Hur, *Phys. Rev. A* **86**, 053804(2012).
 - ¹⁷ B. Bauer, L. Cincio, B. P. Keller, M. Dolfi, G. Vidal, S. Trebst, and A. W. W. Ludwig, *Nat. Comm.* **10**, 1038 (2014).
 - ¹⁸ A. O'Brien, F. Pollmann, and P. Fulde, *Phys. Rev.* **B81**, 235115(2010).
 - ¹⁹ F. Pollmann, P. Fulde, and K. Shtengel, *Phys. Rev. Lett.* **100**, 136404(2008).
 - ²⁰ I. Martin and C. D. Batista, *Phys. Rev. Lett.* **101**, 156402.
 - ²¹ Li Tao, *Eur. Phys. Lett.* **97**, 37001(2012).
 - ²² W. S. Wang, Y. Y. Xiang, Q. H. Wang, F. Wang, F. Yang, and D. H. Lee, *Phys. Rev. B* **85**, 035414 (2012).
 - ²³ R. Nandkishore, L. S. Levitov, and A. V. Chubukov, *Nat. Phys.* **8**, 158(2012).
 - ²⁴ M. Kiesel, C. Platt, W. Hanke, D. A. Abanin, and R. Thomale, *Phys. Rev. B* **86**, 020507(2012).
 - ²⁵ S. L. Yu and J. X. Li, *Phys. Rev. B* **85**, 144402 (2012).
 - ²⁶ M. L. Kiesel and R. Thomale, *Phys. Rev. B* **86**, 121105(R) (2012).
 - ²⁷ W. S. Wang, Z. Z. Li, Y. Y. Xiang and Q. H. Wang, *Phys. Rev. B* **87**, 115135 (2013).
 - ²⁸ M. L. Kiesel, C. Platt, and R. Thomale, *Phys. Rev. Lett.* **110**, 126405 (2013).
 - ²⁹ M. Zhou, Z. Liu, W. M. Ming, Z. F. Wang, and F. Liu, *Phys. Rev. Lett.* **113**, 236802 (2014).
 - ³⁰ Y. Y. Xiang, W. S. Wang, Q. H. Wang and D. H. Lee, *Phys. Rev. B* **86**, 024523 (2012).
 - ³¹ W. S. Wang, Y. Yang and Q. H. Wang, *Phys. Rev. B* **90**, 094514 (2015).
 - ³² D. Wang, W. S. Wang and Q. H. Wang, *Phys. Rev. B* **92**, 195102 (2015).
 - ³³ A. P. Schnyder, S. Ryu, A. Furusake, and A. W. W. Ludwig, *Phys. Rev. B* **78**, 195125 (2008).
 - ³⁴ Q. H. Wang, C. Platt, Y. Yang, C. Honerkamp, F. C. Zhang, W. Hanke, T. M. Rice, and R. Thomale, *EPL*, **104**, 17013 (2013).